New Method for Calculation of Average Electric Properties of Reference Head Phantom in Microwave Imaging

Tushar Singh[1,2], Branislav Ninkovic[1], Miodrag S. Tasic[2], Marija Nikolic Stevanovic[2], Branko Kolundzija[1,2]
[1]WIPL-D d.o.o. Belgrade Serbia, branko.kolundzija@wipl-d.com
[2]School of Electrical Engineering, University of Belgrade, Belgrade, mnikolic@etf.rs

Microwave imaging has many applications in the biomedical area, and one of the most promising application is brain stroke detection. The full-wave 3D modeling of medical imaging scenarios requires significant computational resources due to the complex anthropomorphic phantoms and antenna systems. Hence, it is of paramount interest to simplify unnecessary details in numerical models, without sacrificing accuracy. Algorithms for reconstruction are based on scattering parameters and electric field in the domain of interest. Hence, by comparing the S-parameters of the original model and the simplified one, we can assess the quality of the simplification. Here, we propose the algorithm for computing the equivalent homogeneous phantom from a realistic human head model. In the qualitative algorithms, the equivalent phantom can be used for the reference model as the patient's head before the stroke onset. In quantitative algorithms, such model can be employed as the intelligent solution for initializing the iterative process.

***Index Terms*—microwave imaging, numerical modelling, averaging techniques.**

I. INTRODUCTION

Brain stroke is one of the leading causes of death in today's world. It occurs when the blood supply to a part of the brain is disrupted or blocked, damaging the brains' tissues. The patient suffering from a stroke requires immediate diagnosis and treatment, which includes distinguishing between the ischemic or hemorrhagic type of stroke. Lack of proper diagnosis and treatment causes neurological impairment or even death [1].

At present, stroke detection relies on standard technologies such as X-Ray, Magnetic Resonance Imaging (MRI), Computed Tomography (CT), and Positron Emission Tomography (PET) [2]. These imaging methods provide good spatial resolution and detailed information on tissues but still have several drawbacks. X-ray, CT, and PET use harmful ionizing radiation, which is contraindicated for some patients (e.g., patients with weak kidneys). MRI is non-invasive, but it requires expensive and non-portable equipment. PET and CT diagnostic systems are also costly. They can be portable, but they are not appropriate for bedside monitoring due to their huge size. On the other hand medical microwave imaging (MMWI) has emerged as an alternative tool to the imaging technologies mentioned earlier for brain diagnostics [3], [4]. The advantages of microwave imaging over conventional technologies are low cost, usage of non-ionizing radiation, low health risk, and non-invasiveness.

In order to design, test, and develop a medical device based on microwave imaging, there is a requirement for a powerful three-dimensional (3D) EM simulation environment. Such a simulation tool should provide both ease of modeling and efficient numerical analysis. Microwave imaging scenarios consist of complex anthropomorphic phantoms and realistic measurement systems. Thus, numerical analysis of such systems is still a challenging task due to many unknowns. Hence it is of interest to simplify the phantom while preserving the simulation accuracy.

Realistic human phantoms also have an indispensable role in the development of imaging algorithms. For example, in differential microwave imaging [5], we look for changes in tissue properties with respect to the previous measurements. Most often, this previous state is only vaguely known. Hence, most algorithms use the "average head" to model the patient's head before the stroke onset. However, there is no clear strategy for computing this equivalent homogeneous model. On the other side, quantitative algorithms, such as the distorted Born iterative algorithm [6], aim to restore the complex permittivity distribution in the whole domain of interest. However, due to inverse scattering problems' inherent ill-posedness and non-linearity, this is a problematic task prone to false solutions. The convergence of the solution is highly dependent on the initial estimate. A smartly chosen homogeneous model, used for the initialization of the iterative algorithms, can improve the solution convergence and mitigate the occurrence of erroneous solutions.

We present a novel approach for obtaining the average permittivity of the human head phantom, which can serve as a reference model for qualitative imaging and initial guess for the quantitative algorithms. Investigations show that stroke majorly occurs in the upper half of the head [7]. Thus we consider the model with seven most important tissues: skin, fat, mucous membrane, skull, white matter, grey matter, and cerebellum [8]–[11]. We compute the equivalent homogeneous phantom using different mixing formulas [12] and compare the scattering response of such a system with that of the original phantom. Finally, we use the average permittivity, which yields the slightest error as the initial value for the gradient optimization algorithm to reduce the error further.

The paper is divided into four sections. In section II, we give a brief description of the microwave imaging system

aimed for head imaging. Section III describes different averaging techniques. Section IV presents numerical results obtained after averaging the original inhomogeneous head model. Finally, section V concludes the paper.

II. Medical Microwave Imaging Scenario

In cooperation with NEVA (bio) Electromagnetics [13], the 3D EM simulation platform WIPL-D Pro [14] provides accessibility to anatomically accurate human models for electromagnetic simulations of various complexities. These models consist of a large number of STL files associated with different organs and tissues. Here, we use a female head model ("Static VHP-Female model v2.2 of NEVA Electromagnetics") consisting of seven tissues (skin, fat, mucous membrane, skull, white matter, grey matter, and cerebellum).

The phantom was initially defined using an immensely refined triangular STL mesh. In order to obtain a numerically efficient model, we reduced the beginning number of triangles using a controlled decimation [15]. Such triangular phantom is then converted to a quadrilateral mesh for better numerical efficacy. We expressed approximation quality through a parameter called maximum deviation, σ_{max}, representing the maximal Euclidean distance between each node of the original triangular mesh and its projection to the triangular or quadrilateral surface. Fig. 1(a) shows the outer surface of the phantom decimated and meshed with σ_{max} = 3 mm. Fig. 1(b) shows the interior of the phantom. The complex permittivities of the selected tissues at 1 GHz are shown in Table I.

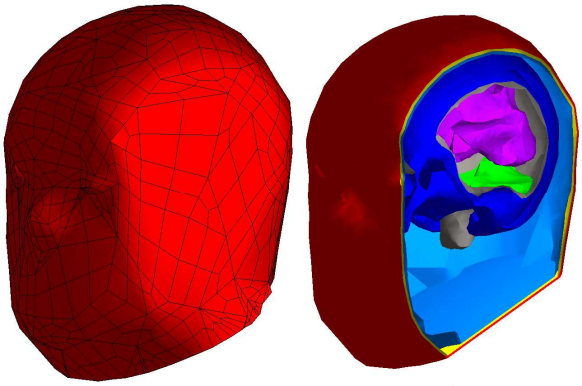

(a) (b)

Fig. 1. (a) Meshed outer surface of the head phantom. (b) Interior of the head phantom.

TABLE I. Electrical Properties of Tissues

No.	Tissue Name	ε'	ε''
1	Skin	45.7110	15.8437
2	Fat	11.2943	2.09200
3	Mucous Membrane	45.6618	15.9454
4	Skull Bone	20.5839	6.5422
5	White Matter	38.5839	11.1790
6	Grey Matter	52.2823	17.7132
7	Cerebellum	48.8582	23.5123

The complete microwave imaging scenario involves realistic antennas placed in the vicinity of the phantom. In the past, different types of antennas were developed for microwave imaging [16]. Here we use the optimized and well-matched microstrip trapezoidal patch antenna (MTPR), as shown in Fig. 2. The antenna was designed on FR-4 substrate and fed with a coaxial cable. Using 21 MTPR antennas, we developed a measurement system in the shape of a helmet, represented in Fig. 3. The antennas in the helmet were closely packed near the phantom to maximize the signal transmission through the phantom tissues, as shown in Fig. 4.

A numerical simulation of the presented scenario is still a challenging task, requiring a long execution time. Each tissue is a complex identity by itself, and seven tissues sum up to an even more complex structure, as given in Fig. 5 (a). In order to reduce the complexity of the system, we look for an equivalent homogeneous phantom filled with the average tissue, as shown in Fig. 5(b).

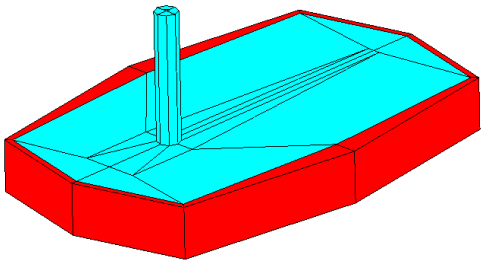

Fig. 2. Microstrip trapezoidal patch antenna (MTPR).

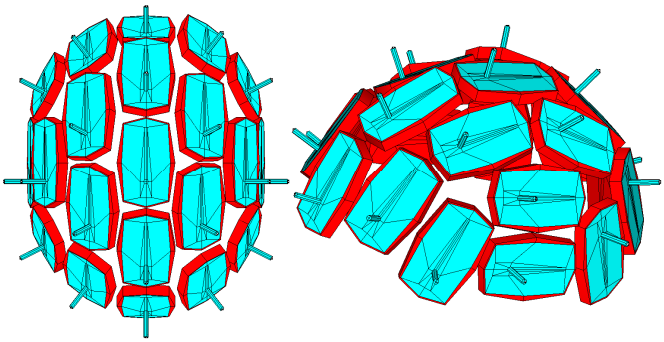

Fig. 3. Measurement system: helmet of MTPR antennas.

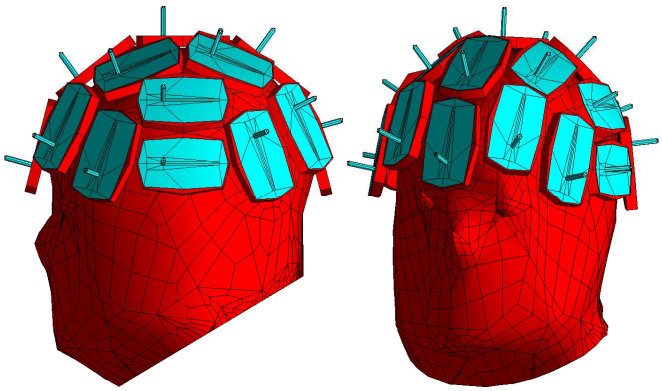

Fig. 4. Head phantom with 21 MTPR antenna helmet.

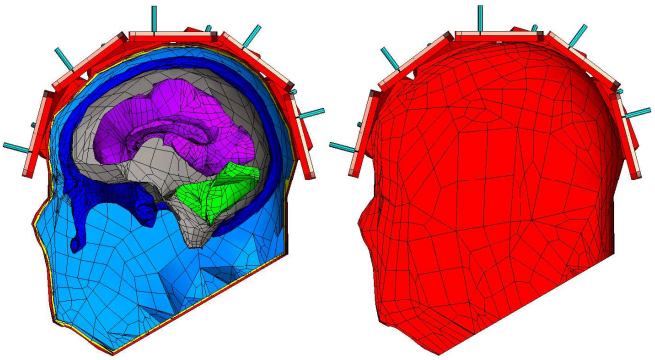

(a) (b)

Fig. 5. (a) Original head phantom with seven tissues. (b) Homogeneous head phantom filled with the average tissue.

III. Averaging Method for Reference Head

To determine the average head complex permittivity, we need to compute the volumes occupied by each tissue. We divide the head's interior into a grid of uniform voxels, and for each voxel, determine to which domain it belongs. By summing the voxels belonging to the same domain, we compute the volume for each tissue. We study three different averaging techniques: the standard averaging, Lichtenecker mixing formula, and Looyenga mixing formula [12].

1) Standard averaging procedure: The average permittivity is obtained as

$$\varepsilon_{\text{avg}} = \frac{1}{V}\sum_{i=1}^{N} v_i \varepsilon_i \,, \tag{1}$$

where v_i is the volume occupied by the ith tissue, N is the total number of tissues, and V is the total volume of the head, i.e., $V = \sum_{i=1}^{N} v_i$.

2) Lichtenecker mixing formula: This formulation involves the logarithms of complex tissues permittivities

$$\varepsilon_{\text{avg}} = \exp\left(\frac{1}{V}\sum_{i=1}^{N} v_i \ln(\varepsilon_i)\right), \tag{2}$$

and it is used in mixing biological materials such as human blood [17].

3) Looyenga mixing formula: This technique utilizes exponentials of complex tissue permittivities

$$\varepsilon_{\text{avg}} = \left(\frac{1}{V}\sum_{i=1}^{N} v_i \varepsilon_i^{1/M}\right)^{M} \tag{3}$$

where $M = 1,2,\ldots$ Looyenga mixing formula is widely used in mixing liquid materials for developing physical phantoms [18]–[19].

To measure the approximation quality, we define a relative root-mean square (RMS) deviation, δ

$$\delta = \frac{\sum_{i=1}^{21}\sum_{j=1}^{21}\left|\Delta S_{ij}^{\text{exact}} - \Delta S_{ij}^{\text{hom}}\right|}{\sum_{i=1}^{21}\sum_{j=1}^{21}\left|\Delta S_{ij}^{\text{exact}}\right|}, \tag{4}$$

as a measure of discrepancy between the scattering parameters of the exact (inhomogeneous) model and the scattering parameters of the approximate (homogenous) models.

After selecting the complex permittivity with the smallest deviation, we use this value to initiate the gradient optimization method. The gradient method also uses δ as the cost function and has two unknown variables - the real and imaginary part of the average complex permittivity.

IV. Numerical Results

In this section, we present the numerical results for computing the average permittivity of the reference head. Table II shows the results for the volume fractions of each tissue. The obtained values for the complex permittivity of the average head and the corresponding deviation, δ , are given in Table III.

TABLE II. Relative Volumes Occupied by Head Tissues

No.	Tissue Name	Volume fraction v_i / V[%]
1	Skin	5.1228
2	Fat	7.3746
3	Mucous Membrane	50.8728
4	Skull Bone	10.3113
5	White Matter	5.5376
6	Grey Matter	19.1656
7	Cerebellum	1.6162

TABLE III. Average Permittivities and the Corresponding Relative RMS Deviations

No.	Averaging Method	ε'	ε''	Relative RMS deviation [%]
1	Normal Averaging	41.47	14.15	16.36
2	Looyenga (M = 2)	40.24	13.56	14.94
3	Looyenga (M = 3)	39.76	13.32	14.42
4	Lichtenecker	38.66	12.76	13.33

As can be seen from Table III, the permittivity computed using the Lichtenecker formula produced the smallest error. Thus, we used this value to initialize the gradient optimization method. The method converged after several iterations, yielding $\varepsilon_r = 34.68 - j12.68$ for the average permittivity with relative error $\delta = 10.97\%$. Fig. 6 shows the magnitude of scattering parameters computed for the original and the average phantom, as well as the magnitude of their difference.

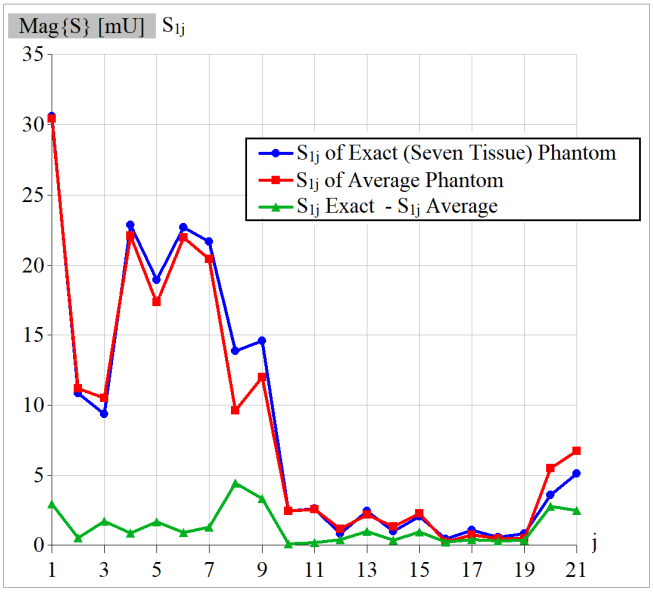

Fig. 6. Scattering parameters (S_{ij}) of the reference head with seven tissues and those of the homogeneous head filled with the average tissue obtained using the gradient optimization method.

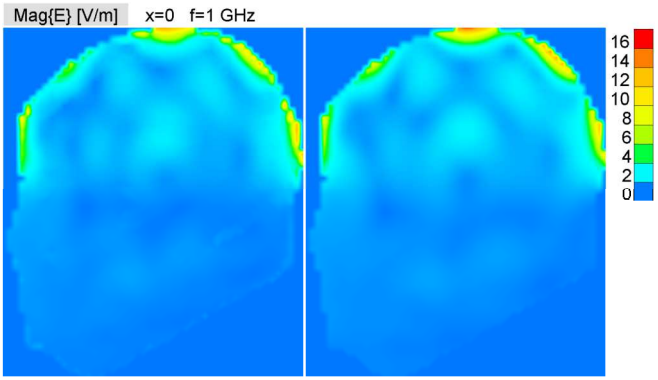

(a) (b)

Fig. 7. Near field analysis: (a) head model with seven tissues and (b) head model filled with the average tissue.

We have also inspected the distribution of the magnitude of the electric field vector inside the phantom. The results from Fig. 7 demonstrate good agreement.

The utilization of the phantom with a single homogeneous medium reduces the execution time by five times (as given in Table IV) and significantly decreases the computational requirement. (The simulations were performed on the desktop machine: Intel i7 920 CPU (2.67 GHz), 32 GB RAM.)

TABLE IV. COMPUTATIONAL TIMES AND NUMBER OF UNKNOWNS

No.	Model	No. of Unknowns	Execution Time [s]
1	Exact Head	60778	627.05
2	Homogeneous Head	24592	140.19

V. CONCLUSION

We have presented a novel approach for computing the equivalent homogeneous phantom starting from the realistic head model with seven tissues. In the process of averaging, we used different mixing formulas such as Lichtenecker and Looyenga. We further improved the obtained results using the gradient optimization method. As the cost function, we used the difference between the scattering matrices of the original and homogenous model. We computed the scattering parameters using a realistic measurement array arranged as a helmet composed of 21 MTPR antennas. Despite the complexity of the original model, the homogeneous model, filled with the average permittivity, yielded an error of the order of 10% for the scattering parameters. The obtained phantom will be helpful in many microwave imaging applications, either as the initial model in the iterative algorithms or the reference model in differential imaging.

ACKNOWLEDGMENT

This work was supported by the EMERALD project funded from the European Union's Horizon 2020 research and innovation program under the Marie Skłodowska-Curie grant agreement No. 764479.

REFERENCES

[1] S. Mustafa, B. Mohammed and A. Abbosh, "Novel Preprocessing Techniques for Accurate Microwave Imaging of Human Brain," in IEEE Antennas and Wireless Propagation Letters, vol. 12, pp. 460-463, 2013.

[2] R. Chandra, H. Zhou, I. Balasingham and R. M. Narayanan, "On the Opportunities and Challenges in Microwave Medical Sensing and Imaging," in IEEE Transactions on Biomedical Engineering, vol. 62, no. 7, pp. 1667-1682, July 2015

[3] .L. Crocco, I. Karanasiou, M. James, R. Conceição, "Emerging Electromagnetic Technologies for Brain Diseases Diagnostics, Monitoring and Therapy, Switzerland, Springer, 2016.

[4] R. Conceição, J. Mohr, M. O'Halloran, "An Introduction to Microwave Imaging for Breast Cancer Detection", Switzerland, Springer, 2018.

[5] M. N. Stevanovic, R. Scapaticci, and L. Crocco, "Three-dimensional sparse microwave imaging for brain stroke monitoring," 12th European Conference on Antennas and Propagation (EuCAP 2018), 2018.

[6] W. C. Chew and Y. M. Wang, "Reconstruction of two-dimensional permittivity distribution using the distorted Born iterative method," in IEEE Transactions on Medical Imaging, vol. 9, no. 2, pp. 218-225, June 1990.

[7] Charlick M, M Das J. Anatomy, Head and Neck, Internal Carotid Arteries. [Updated 2021 Jul 26]. In: StatPearls [Internet]. Treasure Island (FL): StatPearls Publishing; 2021 Jan-. Available from: https://www.ncbi.nlm.nih.gov/books/NBK556061/

[8] A. T. Mobashsher and A. M. Abbosh, "Three-Dimensional Human Head Phantom With Realistic Electrical Properties and Anatomy," in IEEE Antennas and Wireless Propagation Letters, vol. 13, pp. 1401-1404, 2014.

[9] B. Mohammed, A. Abbosh, B. Henin and P. Sharpe, "Head phantom for testing microwave systems for head imaging," 2012 Cairo International Biomedical Engineering Conference (CIBEC), 2012, pp. 191-193

[10] M. Haridim, B. Levin, S. Revich, S. Chulski, R. Sauleau and R. Zemach, "Distribution of energy absorption in an inhomogeneous head model at 900 MHz," in IEEE Electromagnetic Compatibility Magazine, vol. 3, no. 4, pp. 43-48, 4th Quarter 2014.

[11] Joachimowicz, N.; Duchêne, B.; Conessa, C.; Meyer, O. Anthropomorphic Breast and Head Phantoms for Microwave Imaging. Diagnostics 2018, 8(4) p85.

[12] T. Singh, M. Stevanetic, M. Stevanovic and B. Kolundzija, "Homogenization of Voxel Models using Material Mixing

Formulas," 2020 14th European Conference on Antennas and Propagation (EuCAP), 2020, pp. 1-4.

[13] https://www.nevaelectromagnetics.com/

[14] WIPL-D software suite (WIPL-D Pro v17 & Pro CAD 2020), WIPL-D d.o.o, Belgrade, 2020.

[15] T. Singh, S. Abedi, B. Ninkovic, M. N. Stevanovic, N. Joachimowz, H. Roussel and B. Kolundzija, "Smart Simplification of Anthropomorphic Head Phantom Aimed for Microwave Imaging," 2021 15th European Conference on Antennas and Propagation (EuCAP), Düsseldorf, Germany, 2021, pp. 1-4.

[16] T. Singh, M. N. Stevanovic and B. Kolundzija, "Survey and Classification of Antennas for Medical Applications," 2019 13th European Conference on Antennas and Propagation (EuCAP), 2019, pp. 1-5.

[17] Ray Simpkin, "Derivation of Lichtenecker's Logarithmic Mixture Formula From Maxwell's Equations," IEEE Transactions on Microwave Theory and Techniques, Vol. 58, No. 3, March 2010.

[18] S.O. Nelson, "Measurement and Computation of Powdered Mixture Permittivities," Proceedings of the 17th IEEE Instrumentation and Measurement Technology Conference.

[19] Kimmo Kalervo Kärkkäinen, Ari Henrik Sihvola, and Keijo I. Nikoskinen, "Effective Permittivity of Mixtures: Numerical Validation by the FDTD Method," IEEE Transactions on Geoscience and Remote Sensing, Vol. 38, No. 3, May 2000 1303.